

File ID 122468
Filename 5: Longitudinal character of atom-chip-based rf-dressed potentials
Version Final published version (publisher's pdf)

SOURCE (OR PART OF THE FOLLOWING SOURCE):

Type Dissertation
Title Bose-Einstein condensates in radio-frequency-dressed potentials on an atom chip
Author J.J.P. van Es
Faculty Faculty of Science
Year 2009
Pages VIII, 131
ISBN 9789057761867

FULL BIBLIOGRAPHIC DETAILS:

<http://dare.uva.nl/record/292198>

Copyright

It is not permitted to download or to forward/distribute the text or part of it without the consent of the author(s) and/or copyright holder(s), other than for strictly personal, individual use.

5 Longitudinal character of atom-chip-based rf-dressed potentials

Abstract

We experimentally investigate the properties of radio-frequency-dressed potentials for Bose-Einstein condensates on atom chips. The three-dimensional potential forms a connected pair of parallel waveguides. We show that rf-dressed potentials are robust against the effect of small magnetic-field variations on the trap potential. Long-lived dipole oscillations of condensates induced in the rf-dressed potentials can be tuned to a remarkably low damping rate. We study a beam-splitter for Bose-Einstein condensates and show that a propagating condensate can be dynamically split in two vertically separated parts and guided along two paths. The effect of gravity on the potential can be tuned and compensated for using a rf-field gradient.

This chapter has been published as:
J. J. P. van Es, S. Whitlock, T. Fernholz, A. H. van Amerongen and N. J. van Druten
Longitudinal character of atom-chip-based rf-dressed potentials
Phys. Rev. A **77**, 063623 (2008).

5.1 Introduction

Microscopic magnetic traps for neutral atoms and Bose-Einstein condensates (BECs) offer a degree of design flexibility that is unmatched by conventional trapping techniques [49–51]. An ‘atom chip’ typically consists of a lithographically defined wire or magnetization pattern on a substrate to create stable and tailor-made magnetic potentials for controlling atomic motion on the micrometer scale. Already important new applications for atom chips have been demonstrated, including integrated atomic clocks [85], atom interferometers [79, 154–156] and BEC-based precision sensors [70, 131, 132, 157–159], and soon entire networks of atom-optical elements such as atom lasers, single-mode atomic waveguides and atomic beam splitters may be integrated on a single device. The success of atom chips is due primarily to the close proximity of the atoms to the field-producing elements ($\lesssim 100 \mu\text{m}$), which allows high field gradients and small-scale potential landscapes. As a result, atom chips are also versatile tools for fundamental studies of quantum gases in low-dimensions [72, 73] and other exotic potentials.

The flexibility of atom chips is increased further by introducing radio-frequency (rf) oscillating fields to produce rf-dressed adiabatic potentials for atoms [43, 78–81, 101, 160, 161]. This has recently allowed for the coherent splitting of BECs in time-dependent double-well potentials [79, 82], species-dependent microtraps [141], interferometric studies of phase fluctuations in the one-dimensional regime [72], and the direct observation of effects beyond the rotating wave approximation [110].

In this chapter we investigate the properties of atom-chip-based rf-dressed potentials for Bose-Einstein condensates. Previous studies of the *transverse* potential have been made, for example, in the context of double-well BEC interferometry [79, 80, 82], while a recent study on the relative phase evolution of two dressed Bose gases in the one-dimensional regime highlights the importance of the *longitudinal* degree of freedom in atom chip experiments [72]. In general such a rf-dressed potential forms a three-dimensional structure that can be described as a pair of connected waveguides as illustrated experimentally in Fig. 5.1. Using dressed-state rf spectroscopy [110, 162] of Bose-Einstein condensates we characterize and quantify the effect of small magnetic field variations on the rf-dressed potentials, an effect also recently studied for chip-based *time-averaged* magnetic potentials [137, 138]. We demonstrate a significant reduction in the effect of magnetic field noise on rf-dressed potentials and measure an associated reduction of the longitudinal confinement strength indicating that fluctuating homogeneous and inhomogeneous fields are effectively suppressed. The degree of suppression is tuned over one order of magnitude by varying the dressing radio frequency, providing a new handle for tuning the strength of disorder potentials on atom chips. We present experimental results of long-lived longitudinal dipole oscillations of BECs induced in the rf-dressed potentials and find that the damping can be tuned to a remarkably low rate. Further, we realize two y-beam-splitters in a closed loop configuration using the rf-dressed potential. A propagating BEC can be dynamically split in two vertically separated parts and guided along two paths. Finally, we show that the effect of gravity on the symmetry of the potential can be tuned via a rf-field gradient.

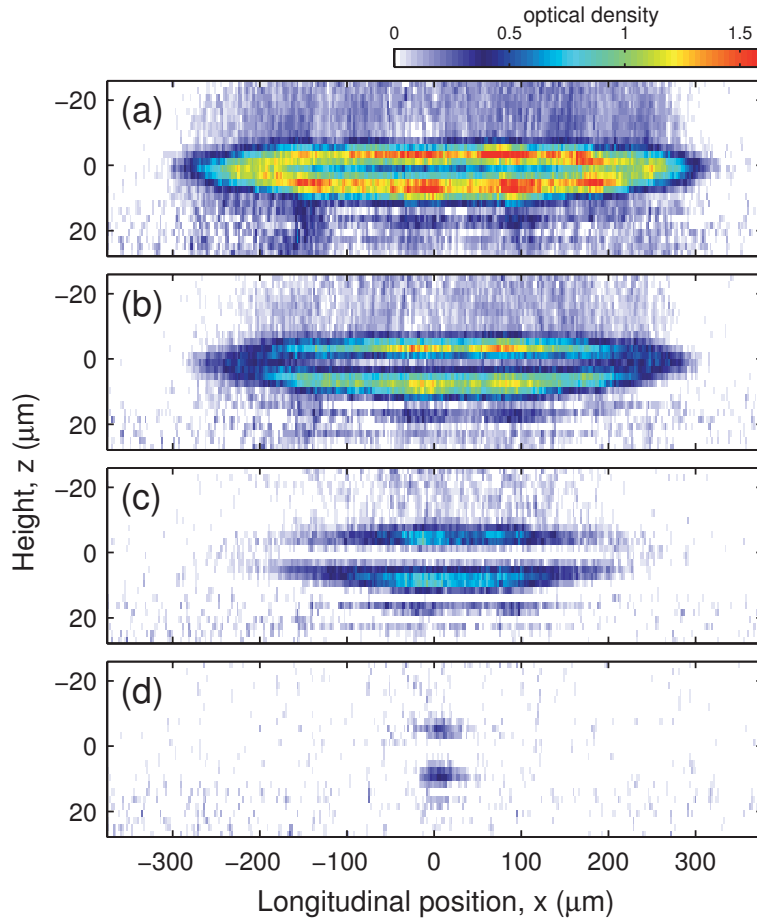


Figure 5.1: Resonant absorption images of ultracold ^{87}Rb atom clouds trapped in a rf-dressed potential. The final temperature of the cloud is varied by varying the final trap depth during evaporative cooling before transferring the atoms to the rf-dressed potential. The final trap depths are (a) $48\ \mu\text{K}$, (b) $29\ \mu\text{K}$, (c) $9.6\ \mu\text{K}$ and (d) $2.4\ \mu\text{K}$. The observed elliptical distribution of atoms results from the longitudinal variation of the character of the dressed potential. Near the center, $x = 0$, the dressed potential forms two parallel waveguides which merge toward the edges of the image at $|x| \approx 250\ \mu\text{m}$.

This chapter is structured as follows. In Sec. 5.2 we provide the equations describing our rf-dressed potential and present a model which accounts for a reduction in the potential roughness. In Sec. 5.3 we describe our experimental setup and the procedures for preparing Bose-Einstein condensates in rf-dressed potentials. In Sec. 5.4 we present and discuss our experimental results. Our findings are summarized in Sec. 5.5.

5.2 Radio frequency dressed potentials

We consider a standard magnetic microtrap (see Fig. 5.2), i.e. the field produced by current through a long wire in combination with an external bias magnetic field

which produce a transverse 2D quadrupole field configuration. Additional wires perpendicular to the first produce a spatially varying field component oriented along the wire to provide approximately harmonic longitudinal confinement. The field components near the magnetic minimum can be conveniently expressed as:

$$\mathbf{B} = \begin{pmatrix} B_x \\ B_y \\ B_z \end{pmatrix} \approx \begin{pmatrix} B_I + c(x^2 - z^2) \\ -qz \\ -qy - 2cxz \end{pmatrix}, \quad (5.1)$$

where $B_I > 0$ is the Ioffe field offset, $c > 0$ is the longitudinal field curvature, and q is the transverse field gradient.

The coupling of a radio-frequency field to magnetically trapped atoms depends on the absolute magnetic-field strength, the rf polarization and on the relative orientation of the static and rf fields. Following [160] and neglecting gravity, in the rotating wave approximation the potential energy experienced by an atom, U , has the simple analytical form

$$U = \tilde{m} \sqrt{(|g_F \mu_B \mathbf{B}| - \hbar\omega)^2 + \hbar^2 \Omega^2}, \quad (5.2)$$

where \tilde{m} is the dressed-state quantum number of the atom, g_F is the Landé g-factor, μ_B is the Bohr magneton, $\omega > 0$ the frequency of the rf dressing field and Ω is the position-dependent Rabi frequency given by the circularly polarized rf-field component referenced to the local direction of the static magnetic field. In this section we restrict our analysis to spatially homogenous and linearly polarized radio-frequency fields with an orientation in the transverse y - z plane. The Rabi frequency is then written as

$$\Omega = \frac{|g_F \mu_B| |\mathbf{b}_{\text{rf}} \times \mathbf{B}|}{\hbar 2|\mathbf{B}|} = \frac{|g_F \mu_B| b_{\text{rf}} \sqrt{B_x^2 + (B_y \sin \theta - B_z \cos \theta)^2}}{\hbar 2|\mathbf{B}|}, \quad (5.3)$$

where \mathbf{b}_{rf} is the radio frequency field with amplitude $b_{\text{rf}} > 0$ and θ is the polarization angle of the radio-frequency field with respect to the y axis. In our experiments we focus on two configurations, namely $\theta = 0$ and $\theta = \pi/2$. For small dressing frequencies the potential is approximately harmonic with a single minimum at $x, y, z = 0$. At a critical radio frequency ω_0 the potential splits into two transversally separated wells. The critical frequency is given by

$$\omega_0 = \frac{|g_F \mu_B|}{\hbar} \left(B_I - \frac{b_{\text{rf}}^2}{4B_I} \right). \quad (5.4)$$

An important quantity is the static magnetic-field strength B_0 at the minimum of the dressed potential. For $\omega \leq \omega_0$ one has $B_0 = B_I$ while for $\omega > \omega_0$, B_0 is the positive solution to the following quartic equation

$$B_0 - \frac{\hbar\omega}{|g_F \mu_B|} - \frac{b_{\text{rf}}^2 B_I^2}{4B_0^3} = 0. \quad (5.5)$$

Note that $B_0 > B_I$ in the latter case, and B_0 depends on the dressing radio frequency, the rf amplitude and the offset field. The transverse positions of the minima are found at $y = 0, z = \pm r_0$ for $\theta = 0$ and at $y = \pm r_0, z = 0$ for $\theta = \pi/2$

$$r_0 = \frac{1}{q} \sqrt{B_0^2 - B_I^2}. \quad (5.6)$$

Specifically, we are interested in the effect of small spatial variations of the longitudinal magnetic field on the smoothness of the rf-dressed potential. This is parameterized as the change in dressed potential energy as a function of a small change in the magnetic field B_I

$$\frac{dU}{\mu dB_I} = \frac{B_I \left[B_0 - \frac{\hbar\omega}{|g_F\mu_B|} + \frac{b_{\text{rf}}^2}{4B_0} \left(1 - \frac{B_I^2}{B_0^2} \right) \right]}{B_0 \left[\left(\frac{\hbar\omega}{|g_F\mu_B|} - B_0 \right)^2 + \left(\frac{b_{\text{rf}}}{2} \frac{B_I}{B_0} \right)^2 \right]^{\frac{1}{2}}}, \quad (5.7)$$

where $\mu = \tilde{m}|g_F\mu_B|$ is the magnetic moment of the trapped atom and B_0 is given by Eq. (5.5) for $\omega > \omega_0$, while $B_0 = B_I$ for $\omega < \omega_0$. The quantity $dU/\mu dB_I$ (plotted as solid lines in Fig. 5.3) is a ratio which relates the change in potential energy in the rf-dressed potential at the minimum to a change in the magnetic field strength B_I . This quantity approaches unity for $\omega \ll \omega_0$ where the dressed potential resembles that of the bare magnetic trap, and decreases significantly above the splitting point. In the limit of large dressing frequency $\omega \gg \omega_0$ Eq. (5.7) reduces to

$$\frac{dU}{\mu dB_I} \approx \frac{|g_F\mu_B| b_{\text{rf}}}{2\hbar\omega}. \quad (5.8)$$

Hence, for large values of ω , $dU/\mu dB_I$ approaches zero and the potential energies at the trap minima become effectively insensitive to small variations of the magnetic field.

5.3 Experimental setup

Our potentials are created using a microfabricated atom chip produced using optical lithography and metal vapor deposition on a silicon substrate (Fig. 5.2). The chip hosts a series of 1.8- μm -thick parallel Z-shaped gold wires with widths ranging between 5 and 125 μm . A current of 1.055 A through the central, 125- μm wide Z-wire in combination with an external bias field of 20 G along y produces an elongated magnetic trap for ^{87}Rb atoms at a position of 120 μm from the chip surface. The magnetic potential is highly elongated with tight transverse confinement ($\omega_{y,z} \approx 2\pi \times 880$ Hz). Current through a macroscopic wire (diameter 0.3 mm) positioned 0.8 mm beneath the chip surface and perpendicular to the Z-wire produces a dip in the potential to provide additional longitudinal confinement ($\omega_x = 2\pi \times 48.5$ Hz). The field strength at the potential minimum is $B_I = 2.86$ G.

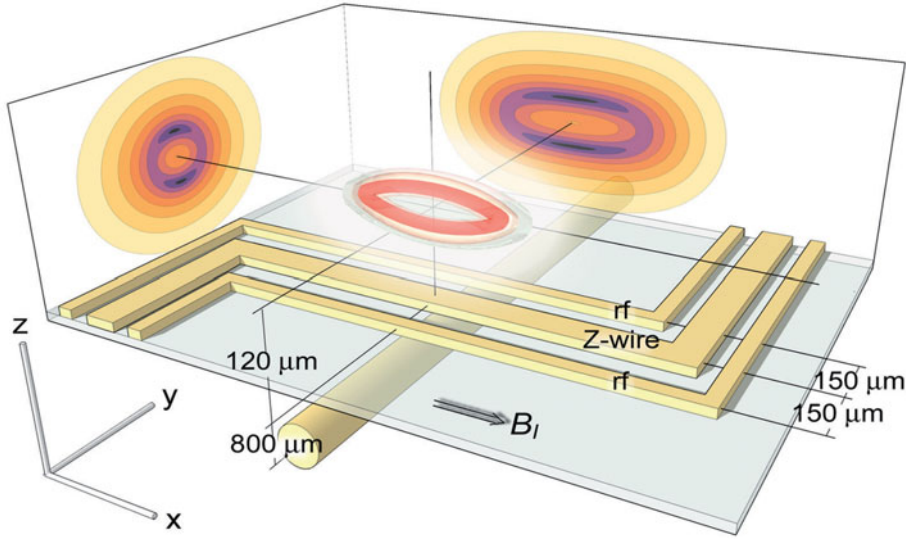


Figure 5.2: Schematic of the atom chip used to produce rf-dressed potentials. The central Z-shaped wire carries a dc current and is used together with an external bias field along y to produce an Ioffe-Pritchard magnetic microtrap. Current through a macroscopic copper wire beneath the chip surface produces a dip in the longitudinal magnetic field (along x) for additional confinement. Positioned next to the Z-wire are two wires which carry rf currents. The amplitudes of the rf currents are controlled to tune the linear polarization angle in the transverse y - z plane, producing either horizontally-split (along y) or vertically-split (along z) rf-dressed potentials. Potential energy cross-sections for vertical splitting are depicted on the back-planes of the image. A sketch of the trapped atom cloud is shown in red.

For these trapping parameters the longitudinal magnetic potential is smooth, with a root-mean-square roughness below our detection sensitivity of ~ 1 mG.

To produce rf-dressed potentials we apply two independent phase-locked rf currents to wires neighboring the central wire on the chip (Fig. 5.2). By varying the relative amplitude of the two currents we precisely control the orientation of the linearly-polarized rf field in the plane perpendicular to the chip wires. For our experiments we create split potentials oriented in both the horizontal y -direction (parallel to the chip) and the vertical z -direction (against gravity). The rf-field strength is tunable and has a typical amplitude of ≈ 1.7 G (1.3 G) for experiments with horizontal (vertical) splitting. In our experiments the Larmor frequency of the atoms is larger than the rf-driven Rabi frequency ($|g_F \mu_B| B_0 / \hbar \Omega \geq 5$) and we neglect the contribution of counter-rotating wave terms to the dressed potential [110]. The rf-field gradient is significant in the vertical direction (≈ 18 G/cm) for vertical splitting and provides an additional spatial dependence used to tune the asymmetry of the potential and to compensate the effect of gravity on splitting.

The typical procedure to prepare a Bose-Einstein condensate is as follows. We start with a cold thermal cloud ($T \approx 1$ μ K) of 1.5×10^5 ^{87}Rb atoms in the $F = 2, m_F = 2$ state in a "bare" static magnetic trap (no rf dressing). To transfer trapped atoms from the static magnetic trap to the rf-dressed potential ($\tilde{m} = 2$) we typically first switch on the rf below resonance ($\omega/2\pi = 1.8$ MHz) and then ramp to the desired dressing frequency between 1 MHz and 4 MHz. At a critical

value of $\omega_0 = 1.82$ MHz (1.90 MHz) for horizontal (vertical) splitting the single potential minimum is split in two. Another weak rf field (≈ 15 mG) is applied to perform forced evaporative cooling in the dressed potential [80, 162]. The trap depth is reduced from 4 μ K to approximately 1 μ K over 350 ms by sweeping the evaporation frequency from 2.36 MHz to 2.33 MHz. After evaporation we are left with an almost pure BEC consisting of 3×10^4 atoms. To image the BEC we typically ramp down the rf amplitude to zero within 20 μ s, and then switch off the static magnetic potential to release the atoms. We use resonant absorption imaging, with the probe oriented along the y -direction (perpendicular to the trap axis, see Fig. 5.2). The typical time-of-flight is 14 ms, the illumination time is 80 μ s and the optical resolution is 4 μ m.

5.4 Experimental results

Shown in Fig. 5.1 is a sequence of absorption images taken of atoms trapped in a vertically split rf-dressed potential for several values for the trap depth. Thermal clouds with different temperatures are prepared in a bare magnetic potential using rf evaporative cooling, where the final evaporation frequency determines the trap depth. The atoms are then transferred to the rf-dressed potential as described in Sec. 5.3, and the dressing radio frequency is linearly ramped from 1.80 MHz to 2.4 MHz in 0.5 s. For final trap depths greater than approximately 25 μ K (corresponding to relatively high-temperature thermal clouds) we observe a distinctive elliptical distribution of atoms which reflects the characteristic shape of the dressed potential. This shape and the observed atomic distribution is due to the inhomogeneous longitudinal magnetic field which introduces a spatial dependence of the rf detuning. Near $x=0$ the potential resembles two parallel waveguides with a vertical separation of approximately 12 μ m. For increasing $|x|$, the local Ioffe field B_x increases and the waveguides approach each other, joining near $|x| = 250$ μ m where the local Ioffe field crosses the critical value defined by the radio frequency [Eq. (5.4)]. As the trap depth and the cloud temperature are reduced further, atom clouds in the two waveguides disconnect and the atoms remain localized at the two minima of the potential.

5.4.1 Effect of magnetic field variations

First we measure the change in potential energy at the minimum of the rf-dressed potential due to a small change in the magnetic field strength B_I oriented along the x -direction (Fig. 5.3). This is measured spectroscopically by probing the energy difference between dressed states of a BEC with an additional weak rf field of tuneable frequency [110]. As the weak rf field is tuned in resonance with the dressed-state level spacing we observe significant atom loss. Changing B_I affects the potential energy of the trapped atoms resulting in a measurable shift of the resonant frequency. The shift is recorded for many values of the rf-dressing frequency and is then compared to the difference in potential energy associated with a change in B_I for a bare

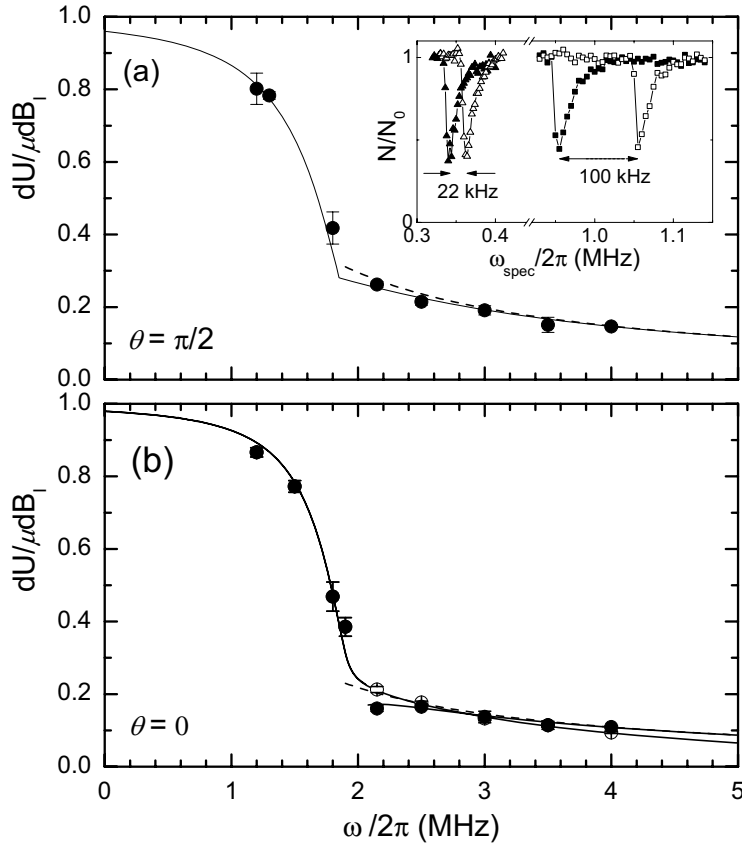


Figure 5.3: The suppressed effect of small magnetic field variations as a function of rf-dressing frequency ω measured using rf spectroscopy of dressed Bose-Einstein condensates. Measurements have been performed for both horizontally split (a) and vertically split (b) potentials. The inset of (a) shows typical rf spectra for two dressing frequencies: $\omega = 2\pi \times 3.5$ MHz (triangles) and $\omega = 2\pi \times 1.3$ MHz (squares) for two values of B_I differing by 0.186 G. The measured suppression ratio $dU/\mu dB_I$ is in excellent agreement with the prediction of Eq. (5.7) (solid lines) and the approximation of Eq. (5.8) (dashed lines) in the limit of large dressing frequency. In (b) we also consider the finite rf field gradient which accounts for the small difference between the two vertically split traps (solid and open circles).

(undressed) magnetic trap.

The experimental procedure is as follows. A BEC is prepared in a rf-dressed potential as described in Sec. 5.3. We linearly ramp the dressing frequency to a desired value at a relatively slow rate of 3.3 MHz/s to minimize excitations. Radio-frequency spectroscopy of the dressed condensate is then performed using a rf pulse, which is weak compared to the rf dressing field ($\sim 0.01b_{\text{rf}}$). The duration of the pulse is adjusted depending on the dressing frequency to remove a large fraction, but not all, of the atoms from the trap at resonance. Typical rf spectra are shown in the inset of Fig. 5.3(a). Each data point corresponds to a new experimental run where the spectroscopy frequency ω_{spec} is iterated over a range corresponding to

$|\omega_{\text{spec}} - \Omega| < 2\pi \times 100$ kHz with a resolution of a few kHz. The width of the resonance is typically $\approx 2\pi \times 10$ kHz and on resonance the spectroscopy field effectively removes about half the atoms from the BEC. For $\omega > \omega_0$ the BEC splits in two spatially separated parts. Because of the vertical rf field gradient, for vertical splitting we measure two resonant frequencies; one associated with each of the two wells. As a result we can selectively out-couple atoms from either well. The resonant frequency provides a measure of the potential energy at the trap minimum for a given value of B_I . To obtain the dependence of the potential energy on B_I for a particular value of ω , we measure spectra for five offset field values around $B_I \approx 2.86$ G each separated by 93 mG. Over this small range the resonant frequency varies approximately linearly with B_I and the slope of a fit to the measurements gives $dU/\mu dB_I$. This procedure is then repeated many times for different values of the dressing radio frequency ω .

A full set of measurements for many values of the rf-dressing frequency and $b_{\text{rf}} = 1.7$ (1.3) G for horizontal (vertical) splitting is shown in Fig. 5.3. For both horizontal and vertical splitting we measure a reduction in $dU/\mu dB_I$ with increasing rf dressing frequency. The solid lines show the expected $dU/\mu dB_I$ based on the theory presented in Sec. 5.2 [Eq. (5.7)] which is in excellent agreement with the experimental results. The dashed lines indicate the simple approximation for $\omega \gg \omega_0$ [Eq. (5.8)]. The kink near $\omega/2\pi \approx 1.85$ MHz corresponds to the splitting point ($\omega = \omega_0$), above which the potential has two minima. Far above the splitting point ($\omega \gg \omega_0$) $dU/\mu dB_I$ decreases as $1/\omega$ [Eq. (5.8)]. Our measurements at $\omega/2\pi = 4$ MHz indicate $dU/\mu dB_I \approx 0.1$, corresponding to a reduction of the sensitivity to magnetic field variations by a factor of ten. This factor can be increased further for even larger dressing frequencies, but is limited in our case by an associated reduction in the coupling strength (due to the changing orientation of the local magnetic field at high dressing frequencies) which leads to non-adiabatic transitions to untrapped dressed states. We expect that much larger suppression factors ($dU/\mu dB_I \approx 0$) could be obtained for dressed-states with $\tilde{m} < 0$ (trapped at the origin for $\omega > \omega_0$ so that $B_0 = B_I$), as Eq. (5.7) then crosses zero near resonance ($\omega = |g_F \mu_B| B_I / \hbar$). This enhanced magnetic field suppression may be the topic of future work.

The effect of magnetic field variations on the trap potential is of particular consequence in magnetic microtraps where spatial variations of the local longitudinal ‘Ioffe’ field cause fragmentation of trapped atom clouds [125, 137, 163]. This effect is suppressed in radio-frequency-dressed potentials which therefore should allow for exceptionally smooth traps and waveguides. However, several additional roughness mechanisms exist in these potentials and their influence should be considered. For example, small magnetic field fluctuations oriented in the transverse y - z direction displace the minimum of the magnetic field and consequently also the position of the rf-dressed potentials. In the case of spatially varying fields this produces small angular deviations of the waveguide axis [125], which for the z -direction gives rise to additional variations of the gravitational potential energy of $2\pi\hbar \times 2.1$ kHz/ μm . We have estimated these effects for our trap parameters. For expected field variations of $\lesssim 1$ mG we anticipate angular deviations of less than 0.2 mrad and vertical displacements of around 10 nm. This corresponds to gravitational potential variations 100 times smaller than the corresponding Zeeman energy shifts ($dU_{\text{grav}}/\mu dB_y \lesssim 0.01$)

and the contribution to the overall potential roughness can thus be neglected as long as $dU/\mu dB_I \gg 0.01$.

In addition to the transverse field dependence, spatial variations of the longitudinal field B_I lead to an additional spatially dependent rf-detuning, which for $\omega > \omega_0$ causes fluctuations of the splitting distance. For vertical splitting this gives rise to an additional gravitational potential which is most significant just above ω_0 , where the splitting distance depends strongly on the local detuning. This effect can be mitigated however if the rf-coupling also depends on the local position in such a way as to compensate the effect of the gravitational potential. In our experiments on vertical splitting, the rf-field gradient in the vertical direction is tuned to precisely compensate the gravitational potential at the splitting point making the total potential energy at the potential minima nearly insensitive to the splitting distance [see Eq. (5.9) in section 5.4.3]. For our parameters this effect therefore plays a negligible role (for all dressing frequencies), peaking at $dU_{\text{grav}}/\mu dB_I = 0.014$ around $\omega/2\pi = 2.5$ MHz. Although these additional roughness mechanisms are approximately an order of magnitude smaller than those probed in the present experiments, they may play a role when higher suppression factors are desired ($dU/\mu dB \lesssim 0.01$).

5.4.2 Longitudinal dipole oscillations

In the previous section we have shown that the effect of magnetic field variations on the rf dressed potential is significantly reduced. To investigate this further we observe the dynamical evolution of BECs propagating in the rf-dressed potential via long-lived longitudinal dipole oscillations. The spatially inhomogeneous field which provides longitudinal confinement is reduced for large rf-dressing frequencies resulting in lower harmonic oscillation frequencies.

Longitudinal dipole oscillations of BECs are produced experimentally by applying a magnetic field gradient along x to displace the potential minimum. The gradient pulse has a cosine temporal profile with a period of 16 ms. The gradient is adjusted to produce oscillations with a roughly constant amplitude between 25 and 50 μm . After inducing the oscillation, we apply an additional weak rf knife above the trap bottom which lowers the trap depth and minimizes heating and the effect of thermal atoms on the oscillations. In all measurements the BEC remains pure within our detection sensitivity for its entire lifetime of approximately 2 s. After various oscillation times we release the BEC and after 14 ms of ballistic expansion we take an absorption image to determine the longitudinal center-of-mass position. The BEC position vs. oscillation time is fit to an exponentially damped cosine function to determine the oscillation frequency and damping time. Shown in Fig. 5.4 are the fitted oscillation frequencies for various values of the rf dressing frequency. The oscillation frequency decreases as expected from the reduced confinement strength, $\omega'_x/\omega_x \approx \sqrt{dU/\mu dB_I}$ (Fig. 5.4-dashed line). Better agreement with the measured oscillation frequency can be obtained by calculating the mean curvature [164] of the rf-dressed potential in the longitudinal direction weighted by the BEC distribution (Fig. 5.4-solid line), which takes into account the small longitudinal anharmonicity of the dressed potential in the vicinity of the splitting point.

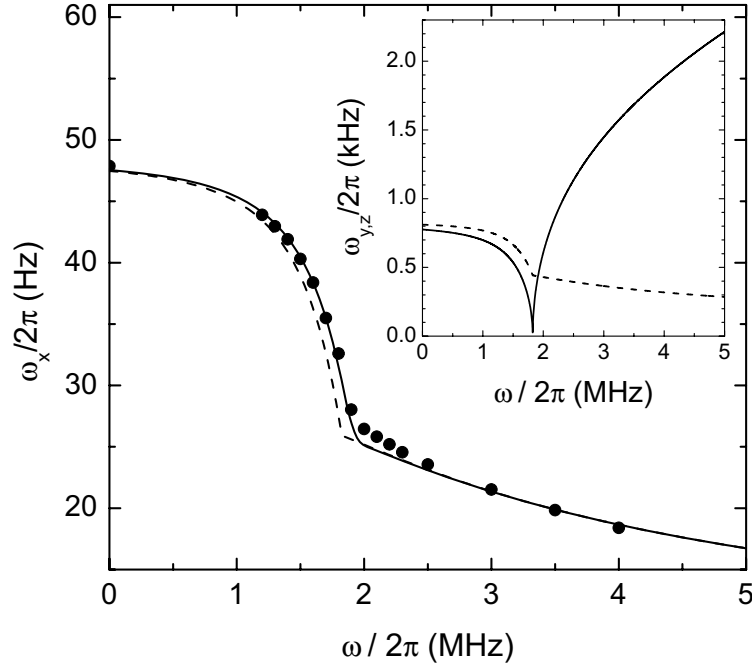


Figure 5.4: Measured longitudinal dipole oscillation frequencies (\bullet) of Bose-Einstein condensates in radio-frequency-dressed potentials. The data is obtained for horizontal splitting and $b_{\text{rf}} = 1.7$ G. The dashed line is the calculated decrease in potential curvature at the trap minimum ($\omega'_x/\omega_x \approx \sqrt{dU/\mu dB_I}$) based on the parameters obtained from the suppression measurements of Sec. 5.4.A. The solid line includes corrections due to anharmonicity of the longitudinal potential which slightly increases the BEC oscillation frequency below resonance. The inset shows the two transverse trapping frequencies (solid line: $\omega_y/2\pi$, dashed line: $\omega_z/2\pi$) calculated as a function of rf-dressing frequency ω .

Our results indicate a significant reduction in the effect of spatially inhomogeneous magnetic fields in rf-dressed potentials.

The transverse confinement is also affected by the rf-dressing fields. The trapping frequencies for horizontal splitting in the two transverse directions are calculated from the curvature of the potential at the minimum (minima) [Eq. (2.28)]. They are shown in the inset in Fig. 5.4. At the splitting point the curvature in the splitting direction goes to zero and the character of the potential is quartic, but is approximately harmonic again for $\omega/2\pi \geq 2.0$ MHz. Note that the rf-dressed potentials are not cylindrically symmetric and for large dressing frequencies ($\omega \gg \omega_0$) each well has three distinct trapping frequencies.

In addition to the oscillation frequency, the damping rates provide a sensitive measure of the properties of the rf-dressed potential. Shown in Fig. 5.5 are the e^{-1} -damping times for longitudinal oscillations obtained from the above fits to the experimental data as a function of the rf dressing frequency. In the bare magnetic trap we observe a damping time of 0.5 ± 0.1 s, significantly less than our obser-

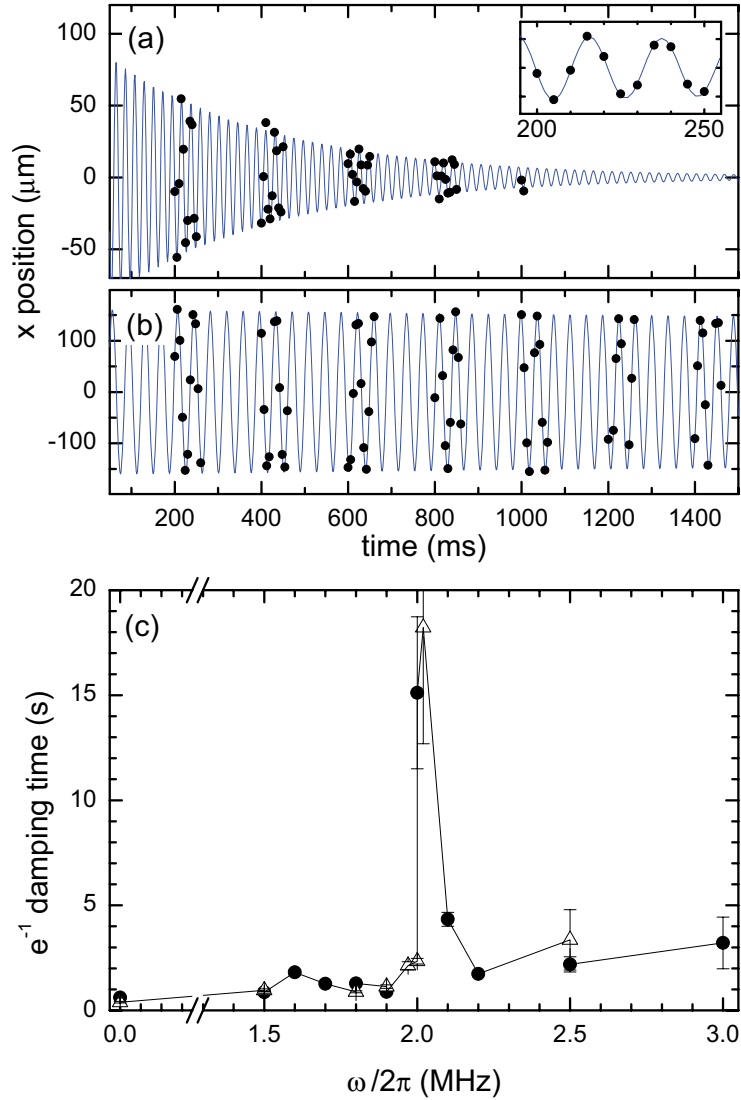


Figure 5.5: Damping of longitudinal dipole oscillations in the rf-dressed potentials. The data is obtained for horizontal splitting. The center of mass position of a BEC as a function of time is recorded after 14 ms expansion for (a) the bare magnetic trap and for (b) a rf-dressed potential with dressing frequency $2\pi \times 2.02$ MHz. The inset of (a) shows a zoomed-in section of the oscillation in the bare magnetic trap. In (c) we show the measured e^{-1} -damping time for various traps as a function of the rf-dressing frequency. The two datasets (circles and triangles) correspond to measurements obtained on two different days.

variations in the rf-dressed trap. Below the splitting point we observe a damping time of 1.2 ± 0.4 s ($\omega < \omega_0 = 2\pi \times 1.85$ MHz), while far above the resonance the damping time is further increased to 2.4 ± 0.8 s. Remarkably, near resonance ($\omega \approx |g_F \mu_B| B_I / \hbar = 2\pi \times 2.00$ MHz) we observe effectively undamped oscillations for the entire lifetime of the BEC consistent with a damping time of >10 s, a fac-

tor of 20 greater than for the bare magnetic trap. Note that at this point the potential is split and the barrier height is sufficiently high to keep the two BECs separated. The exact origin of this sharp decrease in the damping rate remains unclear. One-dimensional numerical simulations of condensates oscillating in our potential have been performed by solving the Gross-Pitaevskii equation for a rough potential (similar to the calculations described in [137] for a thermal atom cloud), but are unable to account for the observations given our trap parameters suggesting a full three-dimensional description is required. The observed damping may be due to the mixing terms in the potential [terms in Eq. (2.23) depending on both x and z] coupling longitudinal motion to the transverse degrees of freedom. To first order these cross-terms can be neglected for $\omega \approx \omega_0$ and this may lead to measurably lower damping rates. Note also that the reduced damping more or less coincides with the point where the two transverse trapping frequencies are equal (cf. inset in Fig. 4).

5.4.3 Beam-splitters for Bose-Einstein condensates

Our results highlight the application of atom-chip-based rf-dressed potentials as smooth atomic waveguides for Bose-Einstein condensates. These potentials can also act as atomic beam-splitters [79,82], necessary components for example in an atomic Mach-Zender interferometer. We have studied both temporal and spatial beam-splitting of stationary and propagating BECs prepared in our rf-dressed potentials. As the dressing radio frequency is increased from below to above resonance, the potential is smoothly transformed from a single well to a double-well potential. Alternatively, one can make use of the spatial dependence of the rf detuning due to the inhomogeneous longitudinal magnetic field. In this case the potential consists of a pair of connected waveguides which merge at the longitudinal extremes (Fig. 5.1).

We perform *temporal* splitting of a BEC in an rf-dressed potential in the vertical z -direction by linearly ramping the rf dressing frequency from 1.80 MHz to 2.05 MHz during a time t_s . The splitting point is between 1.85 MHz and 2.00 MHz depending on the rf amplitude during the splitting process. To split a BEC in equal parts it is necessary to consider perturbations to the rf-dressed potential due to gravity and field gradients caused by the proximity of the trapping wires. In our experiments the presence of an Ioffe field gradient $B'_I = dB_I/dz$ and a rf field gradient $b'_{\text{rf}} = db_{\text{rf}}/dz$ change the symmetry of the rf-dressed potential and together act to compensate for the gravitational asymmetry. To first order the symmetry of the overall potential evaluated at the splitting point ω_0 is given by

$$\left. \frac{dU}{dz} \right|_{\omega_0} = \tilde{m} |g_F \mu_B| \frac{b_{\text{rf}} B'_I + B_I b'_{\text{rf}}}{\sqrt{4B_I^2 + b_{\text{rf}}^2}} - Mg \quad (5.9)$$

where g is the gravitational acceleration and M is the mass of the Rb atom. Equation (5.9) shows that the field strengths and gradients b_{rf} , B_I , b'_{rf} and B'_I can be used to control the symmetry of the potential at the splitting point and therefore also play a role in tuning the splitting ratio for trapped atoms.

In Fig. 5.6 we show the relative number of atoms in each well after time-dependent splitting a BEC in the rf-dressed potential. The symmetry of the po-

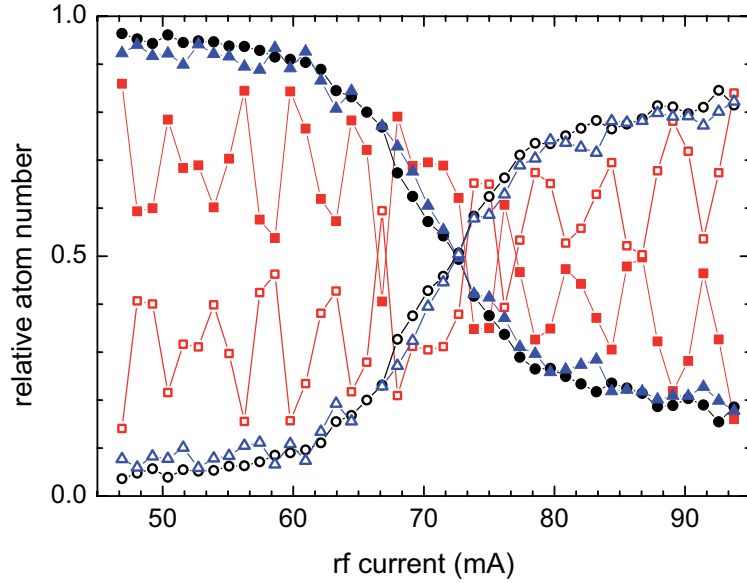


Figure 5.6: Effect of potential gradients on the time-dependent splitting of rf-dressed Bose-Einstein condensates. A BEC is first prepared in a single well and then the dressing radio frequency is linearly increased by 0.25 MHz to split the BEC in the (vertical) z -direction. The rf current is varied to change the rf field strength and gradient thereby tuning the potential symmetry for fixed rf polarization. The rf-field gradient in the z -direction is determined by the wire geometry and is calibrated to approximately 0.25 G/cm per mA. Solid symbols correspond to the population in the lower well, open symbols to the upper well. We observe equal splitting for a rf current of 73 mA ($b'_{\text{rf}} \approx 18$ G/cm) indicating that the effect of gravity can be compensated. Data is provided for three rf-ramp durations t_s of 250 ms (triangles), 75 ms (circles), and 2.5 ms (squares). The complex behavior observed in the 2.5 ms data is most likely due to collective excitations induced during rapid splitting.

tential is controlled by changing the rf currents through the rf wires which affects both b_{rf} and b'_{rf} . The static field is kept fixed with a gradient of $B'_I \approx 74$ G/cm. For long splitting times ($t_s \geq 75$ ms) the atoms follow the global minimum of the split potential. For small rf currents (small b'_{rf}) almost all the atoms of the BEC are measured in the lower well, while for high rf currents (large b'_{rf}) gravity is over-compensated and the upper well is predominately populated. For a critical rf current of 73 mA corresponding to a rf-field gradient of $b'_{\text{rf}} \approx 18$ G/cm we measure equal populations in each well, indicating the potential is symmetric during splitting and the effect of gravity can be compensated effectively. The critical value of b'_{rf} for equal splitting is approximately 10 G/cm higher than expected from Eq. (5.9). We attribute this discrepancy to an uncertainty in determining the physical splitting point for the BEC which (due to the finite chemical potential) occurs for dressing frequencies slightly higher than ω_0 , where the effect of B'_I on dU/dz is weaker [similar to the suppression exhibited in Eq. (5.7)]. We have also measured the splitting ratio for rapid splitting of the potential corresponding to $t_s = 2.5$ ms. In this case we observe less pronounced population imbalances after splitting and a reduced sen-

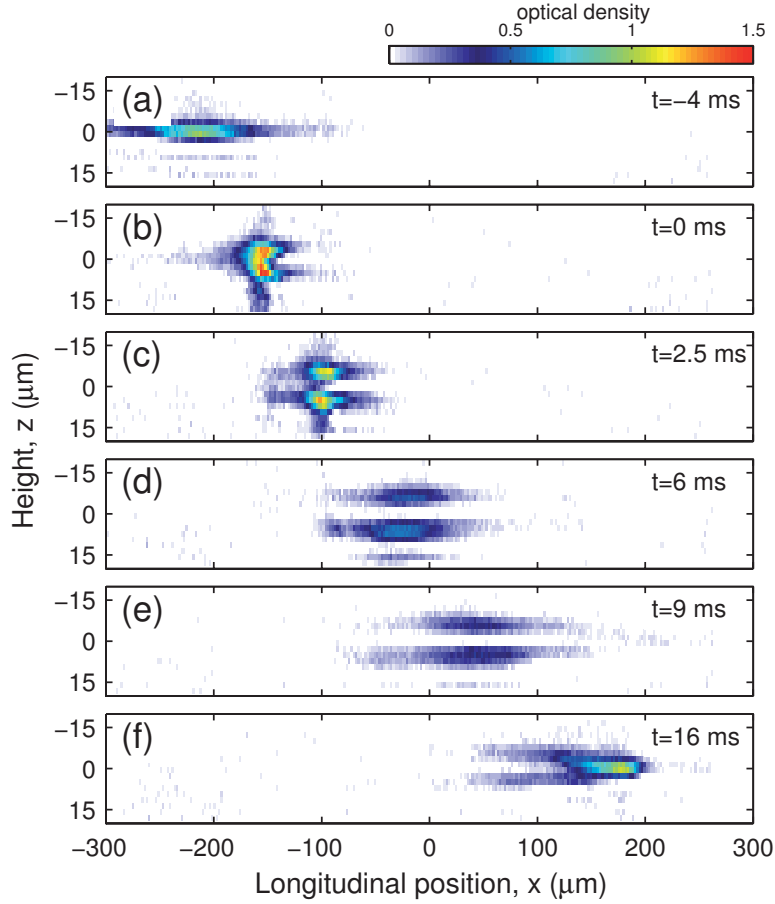


Figure 5.7: A spatial beam-splitter for a propagating Bose-Einstein condensate. In (a) a single BEC is prepared near the edge of the potential by exciting a large-amplitude longitudinal oscillation. At the turning point the parameters of the rf-dressed potential are switched to create a pair of waveguides. The BEC propagates at a velocity of 20 mm/s and is split at a position of $x = -160 \mu\text{m}$ (b). Two parts of the initial BEC propagate in two vertically separated waveguides. About 2 ms after splitting the two BECs are destroyed (see text for details). The two clouds continue moving through the waveguides (c)-(e) and recombine after 16 ms at a position of $x = 160 \mu\text{m}$ (f).

sitivity to the symmetry of the potential. For very short splitting times the final distribution of atoms is expected to become roughly independent of the symmetry of the potential [165]. Additionally we observe complex oscillatory behavior of the final population imbalance presumably caused by collective excitations produced during splitting.

To demonstrate a *spatial* beam-splitter for guided atoms we begin by positioning a Bose-Einstein condensate just outside the split region of the rf-dressed potential. This is performed in a single potential well by rapidly reducing the longitudinal magnetic confinement and displacing the trap minimum by $280 \mu\text{m}$ in the $-x$ direction with a magnetic field gradient. The offset field B_I is also increased. As a result, the BEC begins a slow longitudinal oscillation with a period of approximately 120 ms.

After 40 ms the field gradient is adjusted to position the condensate at a turning point of the new potential at a position of $x = -200 \mu\text{m}$. The applied field gradient is then removed and the longitudinal confinement is increased again within 1 ms. Simultaneously the offset field is returned to $B_I = 2.86 \text{ G}$. The dressing rf frequency is $\omega = 2\pi \times 2.25 \text{ MHz}$ (above resonance) and creates an elliptically shaped potential, cf. Fig 5.1(a).

Under the influence of the increased longitudinal confinement the BEC is accelerated toward the center of the split potential. Absorption images of the BEC taken *in-situ* show the resulting dynamics (Fig. 5.7). After 2 ms of propagation the condensate has a velocity of 20 mm/s and arrives at the splitting point at $t = 0$. We confirm at this point that the BEC is nearly pure with no thermal fraction discernable in absorption images taken after time-of-flight expansion. The shape of the BEC changes dramatically at the splitting point where it separates in two components, each propagating in separate and vertically displaced waveguides. After an additional 2 ms the propagating clouds appear diffuse in time-of-flight images, suggesting that the excitations wipe out the BEC. The two separated components continue to propagate to the end of the potential where they merge. For longer times the cloud reverses direction, is re-split and eventually recombines at $x = -200 \mu\text{m}$ to complete a full oscillation in the rf-dressed potential. To further improve on this result one could try to minimize excitations by reducing the velocity of the BEC. This was not possible in the present work because of the relatively high gradients in the potential outside the split region. Additionally the angle under which the waveguides meet in the splitting point is large, so that the splitting is relatively sudden, probably causing additional excitations.

5.5 Summary and Conclusion

In summary, we have presented a detailed investigation into many relevant properties of radio-frequency-dressed potentials on an atom chip. We have shown that the potential can be described as a pair of parallel waveguides that connect and merge at the ends, highlighting the importance of both the longitudinal and the transverse properties of these potentials.

We have demonstrated theoretically and experimentally using dressed-state radio-frequency spectroscopy, that the effect of magnetic-field noise can be suppressed by an order of magnitude, thereby providing a new handle for tuning the strength of disorder potentials on atom chips. We have studied longitudinal dipole oscillations of Bose-Einstein condensates in the rf-dressed potentials. The frequency of these oscillations is reduced, in agreement with the above suppression. We observe damping times which dramatically increase from 0.5 s to more than 10 s when the dressing radio frequency is tuned close to resonance ($\omega = |g_F \mu_B| B_I / \hbar = 2\pi \times 2.0 \text{ MHz}$). This unexpected result is not fully understood and deserves more attention. Long-lived dipole oscillations allow accurate determination of the trapping potential and are important in novel applications such as precision measurements of forces near surfaces [71].

We have investigated both temporal and spatial beam-splitters for Bose-Einstein condensates using the rf-dressed potentials. We have demonstrated that it is possible to tune the symmetry of the potentials by varying the rf-field gradient. In this way the effect of gravity on beam-splitting is compensated. We have demonstrated that this can alternatively be used to create a highly asymmetric beam-splitter. A propagating Bose-Einstein condensate has been equally split in two parts and guided along two vertically separated waveguides. The splitting is accompanied by excitations that quickly destroy the BEC. We anticipate that this limitation may be overcome using more sophisticated, custom-designed atom chip potentials.

In conclusion, studies of atom-chip-based rf-dressed potentials as presented here, highlight possibilities and opportunities offered by these potentials. The studied rf-dressed potential has a ring geometry which may have applications in rotation sensing and Sagnac interferometry. The present experiments are relevant to a wide range of ultracold-atom systems, such as guided-wave atom lasers [166], one-dimensional gases [72, 73], and interferometers [72, 154].